

High-Resolution Visualization of *Pseudomonas aeruginosa* PAO1 Biofilms by Freeze-Substitution Transmission Electron Microscopy

Ryan C. Hunter* and Terry J. Beveridge

Department of Molecular & Cellular Biology and AFMnet-NCE, College of Biological Science,
University of Guelph, Guelph, Ontario N1G 2W1, Canada

Received 13 July 2005/Accepted 28 August 2005

High-pressure freeze-substitution and transmission electron microscopy have been used for high-resolution imaging of the natural structure of a gram-negative biofilm. Unlike more conventional embedding techniques, this method confirms many of the observations seen by confocal microscopy but with finer structural detail. It further reveals that there is a structural complexity to biofilms at both the cellular and extracellular matrix levels that has not been seen before. Different domains of healthy and lysed cells exist randomly dispersed within a single biofilm as well as different structural organizations of exopolymers. Particulate matter is suspended within this network of fibers and appears to be an integral part of the exopolymeric substance (EPS). O-side chains extending from the outer membrane are integrated into EPS polymers so as to form a continuum. Together, the results support the concept of physical microenvironments within biofilms and show a complexity that was hitherto unknown.

Over the last decade there has been great interest in the study of microbial biofilms because, for many natural prokaryotic communities, this is a preferred natural mode of growth (13). The structural attributes of biofilms have been difficult to study by traditional light microscopic methods (9); these communities are thick (and randomly scatter light), are difficult to image via stains (such as the Gram reaction [6]), and are challenging for phase-contrast microscopy. Confocal scanning laser microscopy has been the preferred method of microscopy because many fluorescent probes are now available and because optical sections can be readily rendered into three-dimensional images with suitable software (43). Indeed, pH discontinuities have recently been demonstrated in biofilms by confocal scanning laser microscopy using a ratiometric fluorescent probe, suggesting the existence of so-called microenvironments throughout the microbial community (30, 65). Yet the use of any optical microscopy has severe resolution limitations for discerning the structural makeup of individual biofilm cells and their surrounding exopolymeric substance (EPS) matrix. Even such high-resolution instruments as atomic force microscopes cannot contribute much to the structural elucidation of biofilms since EPS is too soft and atomic force microscope cantilever force constants are too high for accurate imaging.

For high-resolution imaging of such cellular detail in biofilms, we are then forced to use some form of electron microscopy. Scanning electron microscopes have been used with great benefit on biofilms, especially variable-pressure or environmental scanning electron microscopes that can look at specimens under high relative humidity (14), but these microscopes can only image the topography of the communities, leaving

most of the underlying microbial mass unexamined. By far the best means of analyzing the high-resolution structure of intact biofilm communities is by some form of transmission electron microscopy (TEM) (36). Unfortunately most traditional techniques for TEM, such as conventional thin sectioning, are fraught with artifacts since severe preparatory processes first come into play (10). These include harsh chemical fixation using glutaraldehyde and osmium tetroxide, organic solvents (e.g., acetone) for dehydration, and acidic or basic staining agents (e.g., uranyl acetate or lead citrate). This processing initially allowed reasonable general representation of prokaryotic structure and provided the first high-resolution views of biofilms (12, 20). Yet experience has told us that during processing most proteins are reconfigured, many lipids are extracted, and nucleic acids are atypically condensed (7, 56). Biofilms are among the most difficult biological structures to preserve by conventional means and typically result in poorly preserved cells (especially in the interior of biofilms) and collapsed EPS (throughout the biofilm) (10) so that little accurate structural information can be obtained (Fig. 1).

Great advances have been made in the vitrification of cells to better preserve high-resolution structure (16). Here, cells are so rapidly frozen that all molecular motion is instantly stopped and the cells are encased in a noncrystalline “glass” of ice (amorphous or nanocrystalline ice) (10). This physical fixation of cells is so extraordinary that if the cells are thawed they come back to life. Standard freeze-plunging, freeze-plunging with controlled humidity, and high-pressure freezing have advanced freezing rates to the point where tens of micrometers of specimen depth can be vitrified. This increased freezing depth is now suitable for preserving the structure of biofilms.

One cryotechnique that has assisted in the elucidation of bacterial structure is the freeze-substitution technique. When freeze-substitution is applied to gram-positive or gram-negative planktonic bacteria, much better structural detail is seen (22, 24, 25). In

* Corresponding author. Mailing address: Department of Molecular & Cellular Biology and AFMnet-NCE, College of Biological Science, University of Guelph, Guelph, Ontario N1G 2W1, Canada. Phone: (519) 824-4120, ext. 58904. Fax: (519) 837-1802. E-mail: rhunte01@uoguelph.ca.



FIG. 1. *P. aeruginosa* PAO1 biofilm prepared by conventional TEM processing. These micrographs clearly show the heterogeneous distribution of biomaterials such as membrane vesicles (white arrows), cellular detritus (star), and other extracellular polymers. Unfortunately, little information about biofilm structure can be acquired from such micrographs since conventional processing induces features such as membrane artifacts (white arrowheads) and condensed cytoplasmic material (black arrowheads). Additionally, conventional methods fail to reveal the true nature of extracellular polymers that are known exist between cells. Bar = 2 μ m.

gram-negative bacteria, the periplasm is preserved as a so-called periplasmic gel and the chromosomal material of the nucleoid is dispersed throughout the cytoplasm (27, 28). Remarkably, the freeze-substitution method has even preserved the O-side chains of the lipopolysaccharide (LPS) on the outer face of the outer membrane of *Pseudomonas aeruginosa* (41). Even the cell walls of gram-positive cells show more detail; the walls of *Bacillus subtilis* revealed structural aspects of cell wall turnover (24) and mycobacterial walls showed more accurate distribution of their complex polymeric networks (54, 55).

Although there are recognizable problems with the results presented by the freeze-substitution technique as being as close as possible to representing a natural hydrated structure, these are minor and discernible. Some structures, such as membranes and periplasmic spaces, shrink because of the plastic embedment (50, 51). The freeze-substitution technique is, in our opinion, among the best procedures for elucidating prokaryote structure at the present time and it should provide a wealth of new structural data once applied to biofilms.

To this end, freeze-substitution has been used on *Haemophilus influenzae* and the results were promising (67). Unfortunately, many of the freeze-substitution images of this article showed poorly frozen cells with little detail. In addition, *Haemophilus* has rarely been used as a common model biofilm microorganism and *Haemophilus* biofilms are therefore difficult to compare with more frequently used models. In this paper we show our results using the freeze-substitution method on a biofilm of the frequently used model bacterium *Pseudomonas aeruginosa* PAO1.

MATERIALS AND METHODS

Bacterial strains, culture conditions, and biofilm growth. *P. aeruginosa* PAO1 was used throughout this study and was obtained from J. S. Lam (University of Guelph) and was maintained on Trypticase soy agar (TSA, Becton Dickinson). Planktonic cultures were grown in a dilute Trypticase soy broth medium (dTSB) at a concentration of 3 g per liter (1/10th the recommended concentration) at room temperature to late-exponential phase (optical density at 600 nm = 0.6). Cells were washed twice in 50 mM HEPES buffer and were then processed using freeze-substitution.

Biofilms were cultivated in dTSB on sapphire disks (Al_2O_3) that were 50 μ m thick and 1.4 mm in diameter (Leica Microsystems). Sapphire disks were placed in the lumen of silicone tubing (inner diameter = 1.57 mm) and the entire system (medium, tubing, sapphire disks, waste reservoir) was autoclaved prior to inoculation. Once sterile, the tubing was connected to a Manostat Carter multichannel peristaltic pump (Barnant, Barrington, IL) and was preconditioned with medium for 1 h prior to inoculation. At this point, the flow system was inoculated with an overnight culture of PAO1 (optical density at 600 nm = 0.6) through an upstream injection port. After inoculation, flow was arrested to facilitate bacterial adhesion for 1 h. Following attachment of cells to the sapphire disks, flow was resumed and the dTSB was pumped through at a constant rate of 0.1 ml/min for 7 days.

After 7 days of growth, flow was stopped and sterile forceps were used to remove the sapphire disks. They were then placed on Whatman no. 1 filter paper to remove excess culture medium from the underside of the disk, while leaving a thin layer of medium on top of the cells to keep them fully hydrated throughout freezing. sapphire disks were then placed into flat specimen holders (Leica) that were 1.5 mm in diameter. Immediately prior to freezing, a 10% sucrose solution was placed over top of the biofilm to serve as a cryoprotectant (51).

High-pressure freezing and freeze-substitution. (i) **Biofilms.** The sapphire disks were frozen using a Leica EM PACT high-pressure freezer. Once samples were frozen they were maintained under liquid nitrogen (-135°C), and transferred into 2-ml cryovials (Nalgene) containing 2% (wt/vol) osmium tetroxide (OsO_4) and 2% (wt/vol) uranyl acetate in anhydrous acetone (substitution medium). When indicated, other chemical fixatives were tried in the substitution

TABLE 1. EMAFS freeze-substitution regimen

Step	Time (h)	Temp (°C)	Slope (°C h ⁻¹)
T1 ^a	20	−90	10
S1	3		
T2	10	−60	
S2	3		10
T3 ^b	20	−30	
S3	5		10
T4	11	20	

^a Samples frozen at −180°C in the EMPACT were transferred to substitution medium under liquid nitrogen and then placed in the EMAFS, which was precooled to −90°C.

^b The EMAFS unit required two programming steps. One program ended while another started during T3.

medium, such as 0.075% (wt/vol) ruthenium red and 1% (wt/vol) Alcian blue. The vials were placed into a Leica EMAFS unit for substitution. Here, the biofilms were substituted under strictly controlled conditions as outlined below.

(ii) **Planktonic cells.** Planktonic cells were resuspended in a 10% (wt/vol) sucrose solution and were immediately injected via syringe into thin copper specimen tubes (Leica, inner diameter = 350 µm) for freezing. Tubes were high-pressure frozen identically to biofilm samples, but they required trimming into two halves to expose frozen cells to the substitution medium. Tubing halves were then placed in cryovials and were substituted in the EMAFS unit.

(iii) **Freeze-substitution.** Samples were freeze-substituted under controlled temperatures according to the program outlined in Table 1 for a total 72 h. These substitution steps involved alternating between maintaining samples at a constant subzero temperature and periods of gradual warming. Low temperatures prevented large ice crystal formation, whereas the warmer periods encouraged chemical substitution. Once samples reached room temperature, disks/tubes were removed from the EMAFS and were washed carefully in 100% acetone for 10 min. Disks were then covered with a thin layer of Epon resin and were incubated at 60°C overnight. Once polymerized, the resin was removed from the copper holder and the sapphire disks remained embedded in the resin. The blocks were then placed in flat embedding molds and re-embedded in Epon resin at 60°C for 48 h to produce a block shape conducive to thin sectioning. Copper specimen tubes were washed carefully in acetone for 10 min, and were embedded in Epon at 60°C for 48 h.

Conventional embeddings for comparison purposes. Biofilms grown on sapphire disks were enrobed in 2% (wt/vol) Noble agar and placed in 2.5% (vol/vol) glutaraldehyde for 2 h. Blocks were washed twice in HEPES buffer and fixed in 2% (wt/vol) OsO₄ for 2 h, followed by 2% (wt/vol) uranyl acetate staining for 2 h. Blocks were washed twice in HEPES buffer and were dehydrated through a graded ethanol series (25%, 50%, 75%, 95%, and three times at 100%) for 15 min in each solution. Blocks were suspended in a 50:50 ethanol/LR White resin solution for 30 min, followed by 100% LR White for 1 h. Blocks were embedded in gelatin capsules filled with fresh LR White resin, which were then polymerized at 60°C for 1 h.

Transmission electron microscopy. Biofilms prepared by conventional embedding and freeze-substitution were thin sectioned on a Reichert-Jung Ultracut E ultramicrotome. Before thin sectioning, the sapphire disks were peeled away from the Epon, but the biological material remained embedded in the plastic resin and could be sectioned. For planktonic samples, the copper tubes required some trimming so that no copper came into contact with the knife face during sectioning. Sections were mounted on Formvar- and carbon-coated 200-mesh copper grids. To improve contrast, sections were post stained in 2% (wt/vol) uranyl acetate. Electron microscopy was performed on a Philips CM10 transmission electron microscope operating at 80 kV under standard operating conditions. All observations reported in this paper are based on interpretations from 5 to 10 thin sections from numerous biofilm samples.

SDS-PAGE and Western immunoblotting. LPS was prepared from planktonic and biofilm cells as described by Hitchcock and Brown (26). These extracts were separated by sodium dodecyl sulfate (SDS)-polyacrylamide gel electrophoresis (PAGE) (standardized to 25 µg of protein per lane) and the bands were then transferred to nitrocellulose sheets for Western immunoblotting, as described previously (1). I.e., bands were transferred at 100 V for 60 min, washed briefly in Tris-buffered saline (TBS), and placed in blocking buffer (3% skim milk in TBS) for 60 min. Sheets were then rinsed again in TBS and reacted with either N1F10 (anti-A-band LPS) (40) or MF15-4 (anti-B-band LPS) (39) at room temperature

for 2 h and at 4°C overnight. Bound antibodies were washed twice in TBS and labeled with 0.05% (vol/vol) horseradish peroxidase-conjugated goat anti-mouse immunoglobulin antibody in TBS for 2 h at room temperature. The bands were then developed for 20 min in 0.1 M bicarbonate buffer (pH 9.8) containing 0.33 mg ml⁻¹ Nitro Blue Tetrazolium (Sigma), and 0.15 g ml⁻¹ 5-bromo-4-chloroindolylphosphate (Sigma). Development was stopped by rinsing in deionized water.

RESULTS AND DISCUSSION

TEM has allowed significant advances in the understanding of biofilm physiology. These include an increased understanding of infection mechanisms (35), antibiotic tolerance (66, 72), wastewater processes (17), river water communities (45), and biofilm geochemistry (34, 47). In biological samples, however, TEM procedures can result in the distortion of structural information, either through molecular extraction or redistribution, dehydration and/or aggregation of the extracellular polymers, and through thin sectioning. More often than not, the loss of such information cannot be regenerated afterwards, which results in limited information that is difficult to assess. To this end, biofilms present a major challenge to the microscopist, as they are exemplary specimens prone to artifact and inaccurate imaging.

Biofilms are highly organized aggregates of microorganisms typically surrounded by densely packed matrices of extracellular polymeric substances (EPS). Commonly, EPS provides ~85% vol/vol of the space occupied by a biofilm (but this figure widely varies) and the remainder (~15%) consists of bacteria. EPS is not simply made up of so-called exopolysaccharides (since it is much more complex) and includes heterogeneous combinations of polysaccharides, proteins, and minor amounts of lipids, nucleic acids, and other polymers (11, 64, 68). In fact, larger tangible biomaterials such as outer membrane vesicles, flagella, phages, pili, and debris from lysed cells are also present in variable amounts (Fig. 1) (S. R. Schooling, R. C. Hunter, and T. J. Beveridge, unpublished). Though this heterogeneous mixture of compounds and free-existing structures constitutes such a significant proportion of the biofilm matrix, these constituents of bacterial communities remain to be accurately visualized and characterized via TEM.

EPSs are known to be highly hydrated (~97% of EPS mass exists as water) and are thought to alternate physically between gel and liquid states (4). Because of this highly hydrated nature, the extracellular polymers are difficult to observe (little innate electron scattering power) and to preserve (too much water). In conventional preparation regimens, aldehydes (e.g., glutaraldehyde), uranyl contrasting agents, and osmium complexes are unable to adequately cross-link the polymeric components (e.g., polysaccharide-based components such as alginate in mucoid *P. aeruginosa* strains) and bioparticulates into a resilient network mimicking the natural matrix material. As a result, when dehydration is performed (to prepare the sample for plastic embedding), hydration shells surrounding both the polymers and particulates collapse. Polymer fibers (both polysaccharides and nucleic acids) artificially condense, lipids reorganize or are extracted, and proteins are reconfigured. It has been assumed, but never adequately shown using TEM, that these fibrous polymers and particulates form an extensive polymer meshwork throughout the biofilm. Unfortunately, in a conventional embedding we see a distribution of cells with

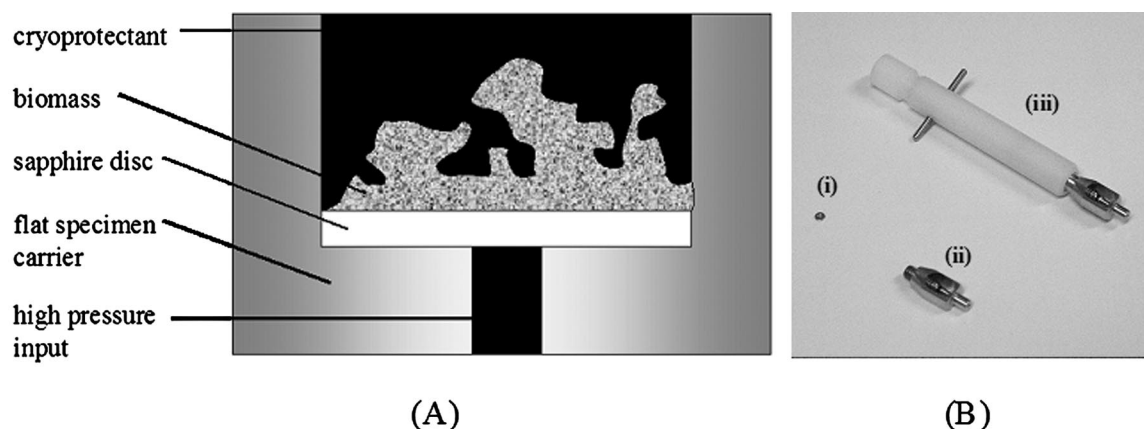


FIG. 2. A) Schematic of the flat specimen holder for freeze-substitution. In short, a biofilm grown on a sapphire disk was briefly dried and transferred to a copper flat specimen carrier. The holder was then filled with a 10% sucrose solution, which served as a cryoprotectant throughout the freezing process. B) The 1.5-mm-diameter specimen carrier (i) was then tightly secured into a loading pod (ii). This entire apparatus was inserted into the high-pressure freezer using a loading rod (iii). Samples were immediately frozen under high pressure, which was applied to the underside of the biofilm substratum as shown in A. An extensive technical description of the high-pressure freezer and the freezing process can be found in Studer et al. (63).

little substance between them (Fig. 1). The cells themselves are poorly represented since their membranes are no longer taut and their DNA has condensed into a central cytoplasmic aggregate.

EPS remains an elusive structure even though it is an important component of biofilms to visualize. This substance certainly plays a role in the chemical (pH, redox and geochemistry of microenvironments) and physical properties (rheology, viscosity, elasticity, penetration barrier, etc.) of biofilms, and in cell physiology (toxicity tolerance, cell-cell signaling, nutrient assimilation, attachment/detachment, etc.). Indeed, the entire concept of there existing so-called microenvironments distributed throughout biofilms relies on there being discontinuities between groups of cells within the overlying matrix. Intuitively, these discontinuities should have subtly different make ups that could be visualized by TEM if they are well enough preserved. Artifacts expressed by conventional embedding have been known for decades (22, 23). Attempts have been made to stabilize, visualize, and identify extracellular polymers through the use of electrostatic cross-linking agents (e.g., multivalent cations), cationized ferritin, and gold-conjugated lectins (3, 29, 31, 32, 33, 38). Though worthwhile, these studies fail to illustrate the true nature of biofilm cells and the EPS that surrounds them.

All aspects of cryo-TEM ultimately rely on the initial freezing step, since cells have to be frozen so rapidly that they are vitrified in amorphous ice. Standard freezing methods, such as plunging samples into a slush of propane held at -196°C (23), can only reliably vitrify ~ 1 to $10\ \mu\text{m}$ of sample depth, which is unsuitable for biofilm studies. Better vitrification occurs at high pressure under low temperatures, thereby ensuring good freezing to depths approaching hundreds of micrometers, and we used high-pressure freezing in this present study (Fig. 2 shows a diagram of the apparatus and explains the process). At high pressure the freezing temperature of water is lowered and the likelihood of undesired ice

crystal nucleation decreases, which is especially important for small particles such as bacteria and their EPS particulates (51).

Figure 3 shows one of our typical freezing data diagrams and indicates that this biofilm sample was cooled at a rate of $1.1 \times 10^4^{\circ}\text{C per s}$ under a pressure of $\sim 2 \times 10^5\ \text{kPa}$. Such conditions preclude the formation of crystalline ice throughout thick biofilm specimens. Additionally, the thermal conductivity of the sapphire substrata ensures that uniform cooling rates are achieved throughout the samples.

Once frozen, freeze-substitution samples have to be chemically stabilized while cellular water is replaced by an organic solvent before the specimens are warmed to room

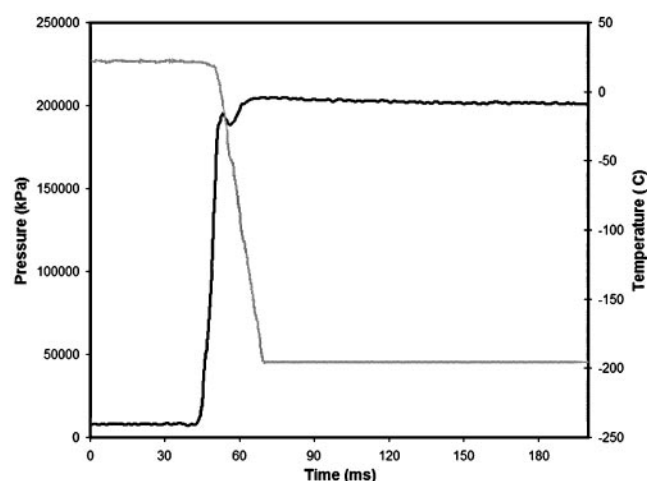


FIG. 3. Typical temperature and pressure changes of the biofilm specimen throughout high-pressure freezing as established by the EMPACT system (Leica Microsystems). This diagram reveals a pressure of over $2 \times 10^5\ \text{kPa}$ (heavy line) was applied, followed by a temperature decrease from 20°C to below -190°C (thin line) at a cooling rate of $1.1 \times 10^4^{\circ}\text{C per s}$. These conditions permit excellent vitrification in specimens up to $\sim 200\ \mu\text{m}$ thick.

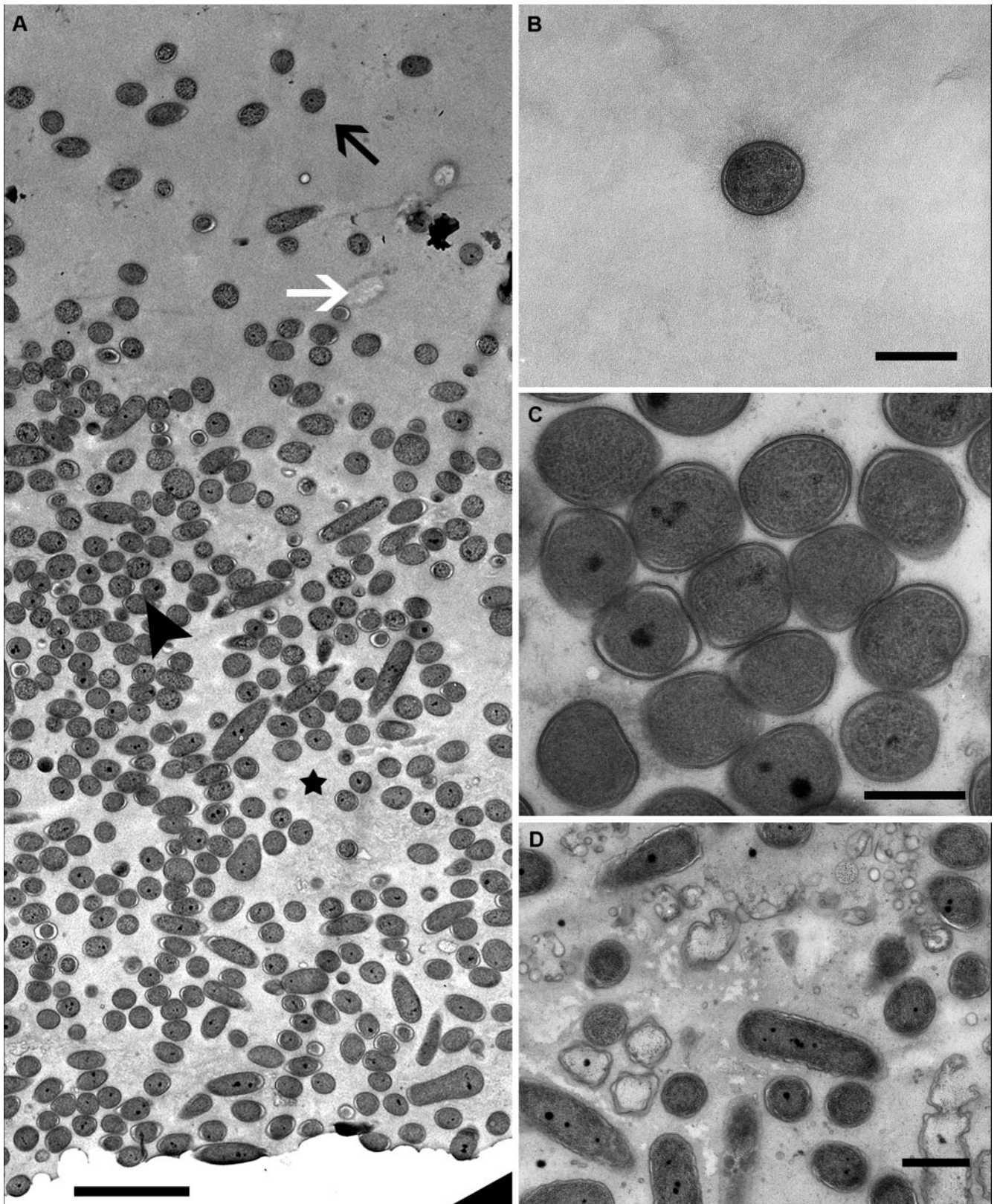


FIG. 4. TEM micrograph of a full biofilm profile in thin section (A), which reveals extensive heterogeneity in terms of cell distribution and physiological status. Prior to sectioning, the substratum was situated at the bottom of the micrograph, while the top represents the biofilm-media interface. Each biofilm shows diffuse (black arrow) and tightly packed cells (arrowhead) with interstitial regions of "void" space (star). A few lysed cells are also visible (white arrow). These characteristics are represented at higher magnification in B, C, and D. B) Cells towards the biofilm-medium interface were few and spread far apart relative to the rest of the biofilm. C) Cells situated away from the biofilm-medium interface were generally tightly clustered and packed along the same axis. D) Some areas adjacent to healthy cells were characterized by extensive cell lysis. These regions appeared to be randomly distributed, but were not found in all biofilms. Bars: A = 5 μm ; B, C, and D = 1 μm .

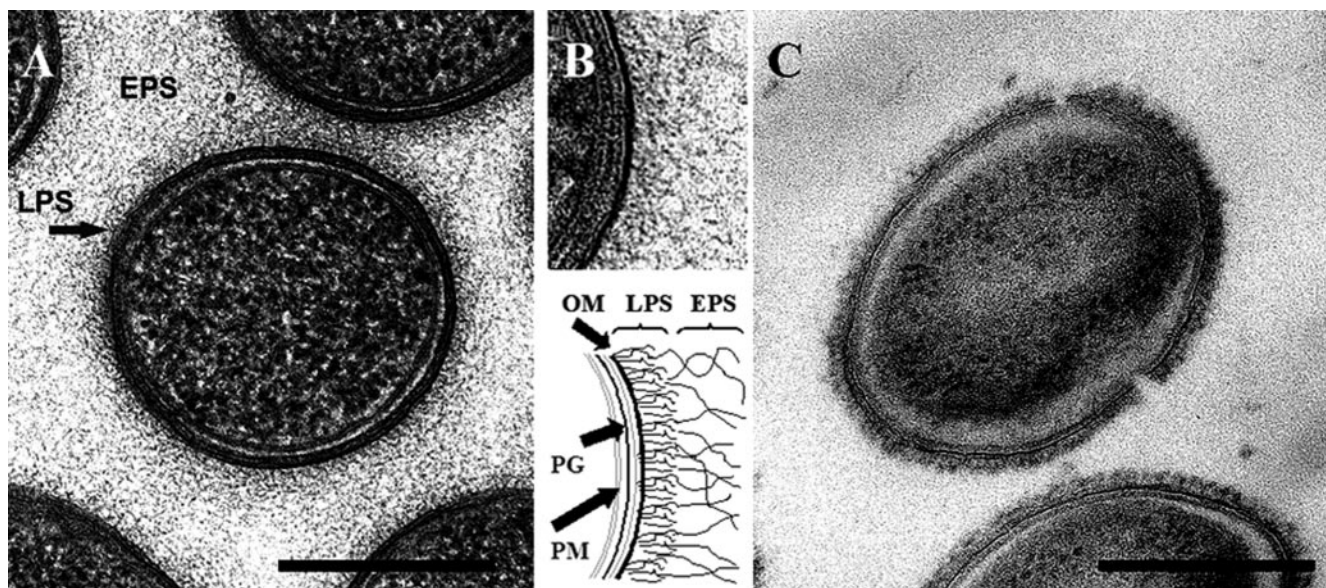


FIG. 5. A) TEM micrograph of freeze-substituted PAO1 biofilm cells. In this image and at higher resolution (B), it is evident that conventional embedding artifacts are not present in these cells, as they are characterized by an evenly stained plasma membrane (PM), a semitranslucent periplasmic gel (PG), a taut outer membrane (OM), and evenly distributed cytoplasm with ribosomes spread throughout. The fibrous background material (EPS) emanating from the lipopolysaccharides (LPS) on the outer membrane is absent from planktonic cells (C), which suggests that these features are the extracellular biofilm matrix. Bar = 0.5 μ m.

temperature so that they can be embedded in plastic for thin sectioning. Over this time, at low temperature (ca. -80°C), biological polymers are cross-linked and stabilized by osmic acid and uranyl ions while in their native (frozen) conformations. Although the action of these chemical agents under low temperature is poorly understood, they are believed to be nonreactive below -90°C (21). However, at such a low temperature, molecules are physically fixed in place, and reactive groups become available for chemical fixatives following a slight rise in temperature. It is also believed, however, that cellular water can recrystallize at slightly warmer temperatures (ca. -80°C), so careful control of substitution temperatures and their duration is vital to successful preservation of biological specimens (P. Hyam, Leica Microsystems, personal communication). Through trial and error, we have worked out a regimen that successfully minimizes cell shrinkage, collapse of delicate polymers, and reorganization of molecular components in *P. aeruginosa* PAO1 biofilms (Table 1).

Figure 4A reveals a full biofilm profile in thin section from the substratum to the bulk fluid interface and represents a full 60 μm of biofilm depth. Higher magnifications of selected regions of the biofilm (from top to bottom) give a better idea of what the cells look like throughout the biofilm community (Fig. 4B to D). These micrographs reveal extensive heterogeneity in terms of cell distribution, a frequently observed characteristic of biofilms through confocal microscopy. Cells towards the biofilm surface were few and spread far apart (Fig. 4A and B), though some pockets of higher cell density were observed as well. Cells in deeper areas of the biofilm were generally observed to be clustered closer together and frequently aligned with one another along the same cell axis (those in Fig. 4C are all cross-sectioned because of this).

Because the cells are enrobed in EPS, mobility is reduced relative to planktonic cultures, and division axes would have a common alignment so that packets of progeny would remain aligned as they grew and divided. This alignment could be beneficial since it provides closer packing of cells and (possibly) easier intercellular communication. Close to these packets of aligned healthy cells, regions of severe cell lysis were also observed (Fig. 4D). This was despite the nutrient-rich growth conditions that the biofilm was under throughout its growth. One would expect that these regions of lysis would become more frequent as the more interior regions of the biofilm were observed, but this was not the case. These lysis regions seemed randomly positioned and were always close to more healthy regions (Fig. 4A). This appears to corroborate suggestions that biofilm microbes are able to survive at the expense of those around them (i.e., an altruistic growth strategy) (37). It should be noted, however, that significant cell lysis was not observed in all micrographs (see Fig. 4A).

Clearly, the areas of the biofilm that are filled with cells and matrix are complex in that packets of cells in many different physiological states are found. Yet, regions of extremely low cell density are also seen in Fig. 4A. We believe these to be voids or water channels, and this would confirm the complex biofilm macrostructure seen by confocal microscopy (44). The sampling area of a thin section is very limited and large macrostructures such as water channels are difficult to interpret but (our) confocal measurements of the biofilms using green fluorescent protein-labeled cells suggested that the biofilms ranged from 60 to 80 μm in thickness. Since this confocal thickness is consistent with that seen with our freeze-substitutions, the biofilm macrostructure seems to be well preserved and these low-cell-density voids must be water channels. Interestingly, measurements of conventionally embedded biofilms

revealed that they had shrunk by ~25% (data not shown). This substantial size difference suggests that quantifying biofilm morphology using cryotechniques is more representative of their natural state.

As previously discussed, conventional embeddings are fraught with artifacts (see Fig. 1) which are not seen in the freeze-substitution samples. High magnification aptly demonstrates this (Fig. 5). Here, the majority of cells have a well-preserved cell envelope that consists of a smooth, evenly stained plasma membrane, a semitranslucent periplasmic gel, and an asymmetrically stained, taut outer membrane (see Fig. 5B for a high-resolution micrograph of the cell envelope). The asymmetry seen in the outer membrane is a reflection of the lipid asymmetry of this bilayer; most LPS resides on the outer face of the membrane whereas most phospholipid is on the inner face. LPS stains darker than phospholipid because of its higher charge density (5). Remarkably, the appearance of the cell envelope approaches profiles observed in frozen hydrated sections viewed by cryo-TEM (51). Here, image contrast is based on mass distribution (i.e., the higher proportion of phosphorus in LPS as opposed to that in phospholipid) of the biomaterial and not on the staining reagents, as in freeze-substitution (56). This confirms how well our freeze-substituted cells have been preserved within the biofilm.

In Fig. 5A the cells look remarkably robust since their cytoplasm is filled with ribosomes and their chromosome is spread throughout the entire cytoplasm; these are structural traits suggesting active metabolic processes and protein synthesis (21, 25, 27, 28, 50, 51). This evenly distributed cytoplasm is in contrast to that seen in the study by Webster et al. (67). These features were surprising since we often naturally assume that many biofilm cells would be under nutrient limitation (no matter the flow rate) and, accordingly, the cells should not look so healthy. Yet studies do suggest strong metabolic activity (57), and recent DNA microarray studies reveal ribosomal gene expression to be upregulated in *P. aeruginosa*, *Escherichia coli*, and *B. subtilis* biofilms versus their planktonic counterparts (60, 62, 69).

It has been suggested that such lines of evidence may be indicative of cells achieving a faster growth rate than expected by enjoying a greater availability of nutrients either through catabolism of the surrounding matrix, or through catabolism of dead cells (46). It is also important to consider that our growth medium (1/10th the recommended concentration of TSB), though dilute, is still extremely rich relative to many natural biofilm environments. Our results indicate that biofilms consist of either pockets of highly active cells (Fig. 5A) or pockets of cell lysis (Fig. 4D) with few cells at intermediate metabolic rates. We did not find that our cells suffered from freezing damage near the base of the biofilm as was previously shown (67).

As comparison for our biofilm study, we also freeze-substituted planktonic cells of PAO1. These were also well preserved and possessed most of the cellular attributes seen in the biofilm bacteria (cf. Fig. 5A and C). The most apparent difference was seen with the contrast of the background of both samples; the biofilm cells had a darker pebbly background whereas the planktonic cells had little background at all. Careful observation of the biofilm cells revealed that most background material was closest to the cell surfaces and that the outer membrane surface possessed fibers emanating from it (Fig. 5A and

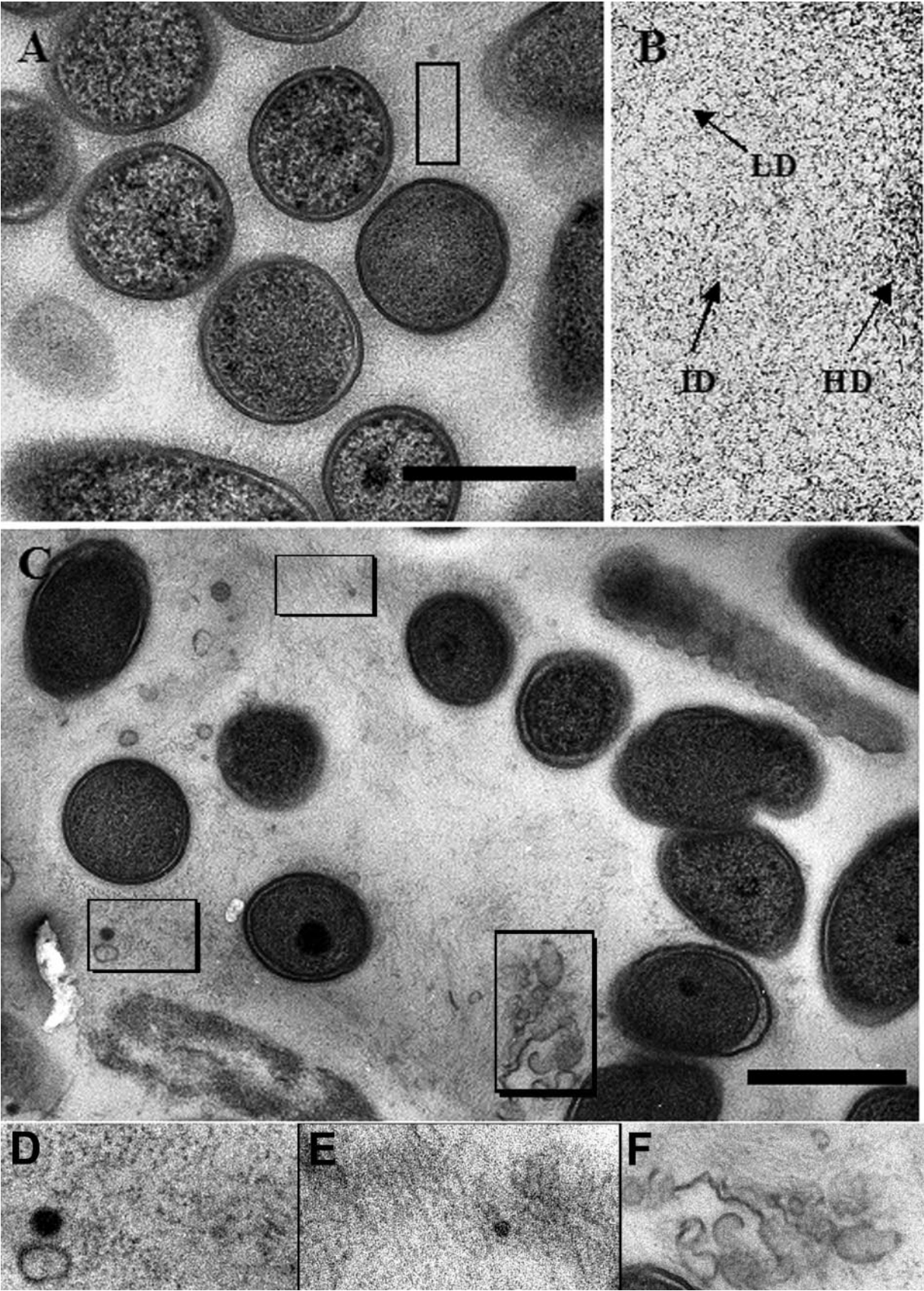
B). Since these structural features were only seen in the biofilm samples, it was apparent that they were associated with the extracellular matrix and that this was the EPS.

Figure 6 reveals this in more detail. Here a close-up of the matrix is taken from a midpoint between two cells (Fig. 6A) to show the granularity of the EPS (Fig. 6B). Obviously, much of this granularity could be due to the staining complexes associated with the EPS, but one certainly gets the impression of high density versus low density polymeric regions (Fig. 6B). In conventional embeddings, various attempts have been made to stabilize acidic extracellular polymers through electrostatic cross-linking using fixatives such as ruthenium red (48) and Alcian blue (61), which are both electron dense and add contrast to the specimen. These attempts have been somewhat successful with other organisms (33, 71), but by their very nature (being multivalent cations) they can artificially condense polymeric materials. No previous successful observations have been reported for *P. aeruginosa*. Here, through freeze-substitution, we reveal fine detail within the EPS polymers without the aid of these extraneous cross-linking agents.

Furthermore, in our study, the EPS surrounding cells adjacent to the substratum was found to be much more heterogeneous than that in other regions of the biofilm. Figures 6C to F reveal at least three distinct configurations of EPS polymer arrangement, if not distinct polymeric types. In Fig. 6C, there is one lysed cell, some membranes (presumably from another lysed cell), and some membrane vesicles, which together emphasize the particulate nature of some EPS components. This is a common trait seen in all regions of the extracellular matrix and emphasizes the extreme complexity of the EPS. Some of these features are shown at higher magnification in Fig. 6D to F. The complexity shown in these micrographs could clearly, at least in part, be responsible for the physical and chemical discontinuities seen throughout a single biofilm, which manifest themselves as microenvironments (30).

Unfortunately, the exact chemical nature of PAO1's EPS still remains to be fully characterized. A recent study describing the EPS of PAO1 biofilms identified the major carbohydrate moieties in this to include glucose, rhamnose, mannose, xylose, 3-deoxy-D-manno-oct-2-ulosonic acid (KDO), *N*-acetylgalactosamine, *N*-acetylglucosamine, and *N*-acetylglucosamine (70). More recently, two genetic loci (*psl* and *pel*) responsible for the production of mannose-rich (*psl*) and glucose-rich (*pel*) polymer components of *P. aeruginosa* EPS (18, 19, 52) were identified. With the exception of KDO with its ionizable carboxylate, most of the sugars described in these studies are neutrally charged or sugars with a possible ionizable amine group (depending on polymeric linkage), which may be difficult to stain. Accordingly, most staining of this PAO1 polymeric EPS must be due to the KDO moiety. It also must be remembered, though, that other highly acidic polymers may also be present, such as DNA (11, 52, 68).

The O-side chain of LPS is another polymeric unit that must be considered in our study, since LPS has been implicated in the architecture of *P. aeruginosa* biofilms (58). Its presence affects the attachment of bacteria to a surface (49) and some of the chemical constituents identified in PAO1's EPS are similar to those in the O-side chain as well as in the core oligosaccharide (70). *P. aeruginosa* PAO1 (serotype O5) produces two types of O-side chains, termed A-band and B-band. The



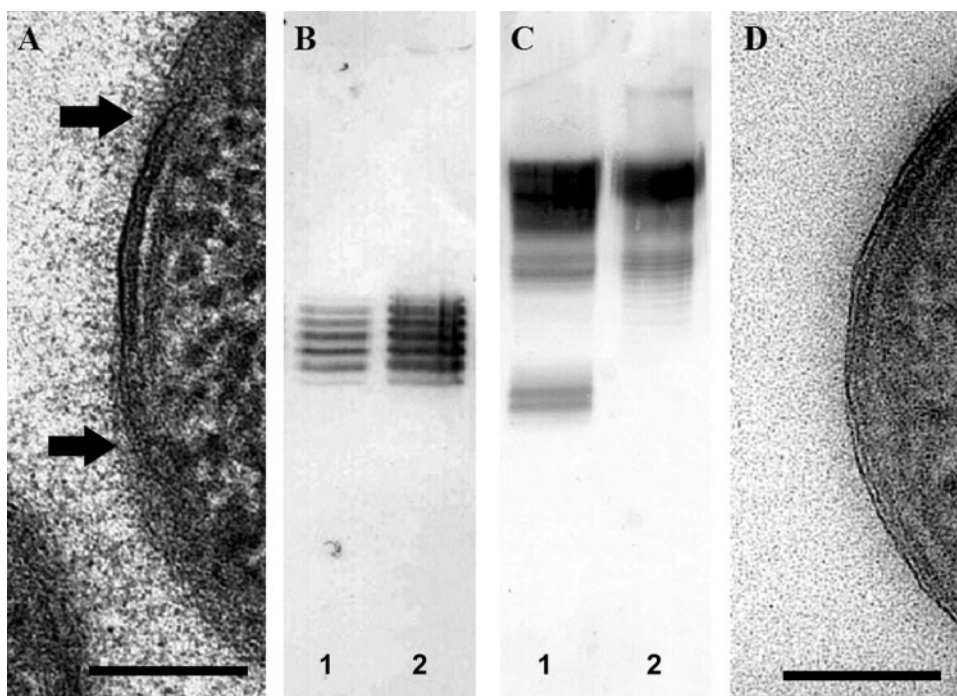


FIG. 7. A) High-resolution image of a biofilm PAO1 cell envelope. LPS can be seen extending from the outer membrane as a fibrous polymer brush (arrows), though it appears to be less electron dense than the surface of planktonic cells (see Fig. 5C). The electron density is likely provided by uranyl ions, which suggests that this polymer is B-band LPS. Bar = 100 nm. B and C) Western immunoblots of LPS isolated from planktonic (lane 1) and biofilm (lane 2) PAO1 cells. SDS-PAGE gels were standardized to 25 μ g protein per lane and reacted with either (B) anti-A band or (C) anti-B band monoclonal antibodies. These blots confirm the presence of B-band LPS in PAO1 biofilms, though it is evident that, relative to planktonic PAO1 cells, B-band is produced in smaller amounts. D) LPS was not visible on several clusters of biofilm cells, which is suggestive of localized microenvironments in which PAO1 alters the characteristics of its cell envelope. Bar = 100 nm.

A-band has a relatively simple, uncharged O-side chain consisting of ~10 to 20 repeating units of a D-rhamnose trimer (2). This neutrally charged polymer is difficult to stain and visualize using TEM (41). The B-band O-side chain is serotype specific and is much more complex.

The B-band O-antigen of the PAO1 strain used in this study (serotype 05) consists of highly charged repeating trisaccharide consisting of two units of β -D-mannuronic acid and one *N*-acetyl-D-fucosamine (35). This polymer is more easily visualized, since the uronic acid residues are able to bind uranyl ions from the substitution medium. If present on biofilm cells, we expected to see the B-band O-side chains as fibrous polymers extending from the outer membrane. Indeed, Fig. 5A and 7A reveal such fibrous polymers on the biofilm bacteria, which suggested the presence of B-band O-antigen. This was confirmed using SDS-PAGE and Western immunoblotting using monoclonal antibodies specific for these two O-antigens (Fig. 7B and C). Both A- and B-bands were present. We were surprised to see these features since Beveridge et al. (8) reported that the A^+B^+

phenotype of PAO1 cells within mature biofilms was displaced by A^+B^- over a 144-h growth period when grown in a chemically defined growth medium.

In our present study, we used a more enriched medium (dTSP), which could explain the difference. Our micrographs (cf. Fig. 5A and 5C) and Western blots did, however, indicate that B^- band LPS was produced in lower amounts than in planktonic cultures, which is similar to results published by Langley and Beveridge (42). Since LPS was not as visible on some cell surfaces in the biofilm (cf. Fig. 7A and D), it is possible that B-band expression is repressed under certain microenvironment conditions, which again reveals the complex heterogeneity within a single biofilm. This is consistent with planktonic studies that have shown *P. aeruginosa* to express these two types of LPS differently under environments of oxygen stress, low pH, high temperature, and various nutrient regimens (53, 59). These results provide further evidence for localized microenvironments throughout *P. aeruginosa* biofilms and may also complement other clinical studies which have shown cystic fibrosis isolates to be A^+B^- (40).

FIG. 6. A) TEM micrograph of a cluster of biofilm cells surrounded by an extensive EPS network. Most EPS is present near the cell surfaces. B) High-resolution image of the EPS region marked in A (see text for details). Microenvironments of EPS of high (HD), intermediate (ID), and low (LD) density are clearly present. C) Some areas adjacent to the substratum reveal more extensive heterogeneity. At least three polymer types or arrangements are present in this small area of the biofilm (outlined) and are shown at higher magnification in panels D, E, and F. While the exact chemical nature of these polymeric configurations is unknown, these micrographs reveal the extensive complexity of the EPS matrix. Bars = 1 μ m.

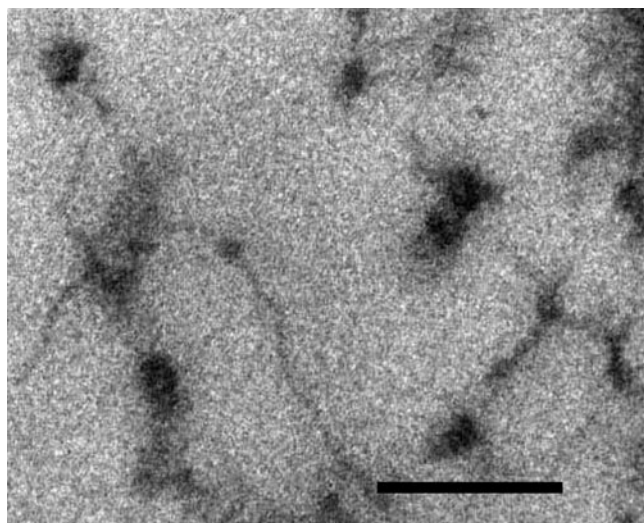


FIG. 8. TEM micrograph of Alcian blue-stained EPS. While this highly positively charged dye provided enhanced contrast of EPS, electrostatic interactions caused condensation of the polymers against each other and against the cells that they surround. Bar = 200 nm.

It was interesting to see that freeze-substitution offered an indistinct line as to where the O-side chains and the EPS met (Fig. 5, 6, and 7). EPS blended into the side chains so completely that it was impossible to ascertain where the side chains ended and where the EPS polymers began. Since chemical analyses suggest that the side chains and the EPS polymers have a common chemical pedigree, it is possible that some of these EPS polymeric fibers are O-side chains that have been excised from LPS molecules. At the same time, when cells were seen in close proximity to each other (Fig. 5, 6, and 7), their O-side chains appeared to intermingle, suggesting a closer union than normally seen with planktonic cells. This could aid intercellular communication between biofilm bacteria.

Numerous combinations of fixatives and solvents were at our disposal for freeze-substitution processing. Graham and Beveridge (23) completed a systematic evaluation of these reagents and found that a substitution medium consisting of osmium tetroxide and uranyl acetate in anhydrous acetone yielded optimal results for planktonic cells. In our study, we found this same combination optimal for PAO1 biofilm cells. The use of gallic acid, glutaraldehyde, or osmium tetroxide and uranyl acetate on their own produced inferior cellular and biofilm preservation (data not shown). Ruthenium red and Alcian blue were tried in the substitution medium, but treatments resulted in either a collapse of biofilm polymers against the cell or the formation of condensed agglomerations on some parts of the fibrils (Fig. 8). This observation has been reported in a previous study (45). Cellular ultrastructure was also inferior when these reagents were used. It is likely that these agents somehow interfered with the action of osmium tetroxide and/or uranyl acetate during substitution.

High-pressure freezing requires the use of a cryoprotectant, which helps organize water molecules during vitrification so as to inhibit ice nucleation on bacterial surfaces that could pierce and lyse the cells (15, 50, 51). For our study we used 10% sucrose as a cryoprotectant, which gave superior results in a

previous cryo-TEM study (51); when it was omitted during freezing, the cells deformed and compressed against each other. It may be argued that a sudden exposure to the cryoprotectant may influence the metabolic activity of the cells or may cause an osmotic effect (which may ultimately change the ultrastructure of the individual cells or biofilm organization). However, since cryoprotectant exposure rarely lasted longer than 20 seconds, we believe this was not possible.

In summary, we have shown that high-pressure freeze-substitution is an extremely rewarding technique to study the natural structure of bacterial biofilms at high resolution. This is especially true for exploring the organization of EPS, since it is kept in a hydrous vitreous state until chemically stabilized. Other cryotechniques could be considered superior for cellular preservation (i.e., frozen hydrated sections [16, 49, 50, 51]), but the density of the EPS polymers is too low in their hydrated state to visualize by that method (V. R. F. Matias, R. C. Hunter, and T. J. Beveridge, unpublished). With the present freeze-substitution study, we provide the first high-resolution view of *P. aeruginosa* biofilm cells and their integration with the surrounding EPS, which is composed of polymeric and particulate substances.

ACKNOWLEDGMENTS

We thank Philip Hyam of Leica Microsystems and Valerio Matias and Dianne Moyles of the University of Guelph for their valuable assistance and technical help. We thank J. S. Lam for providing the PAO1 strain and LPS antibodies and Anu Saxena for her guidance with Western immunoblotting (both at the University of Guelph).

This work was funded by a National Science and Engineering Research Council of Canada (NSERC) Postgraduate Scholarship to R.C.H. and an NSERC-Discovery grant to T.J.B. Some consumables and equipment aspects of this study were funded through an AFMnet-NCE grant to T.J.B. Microscopy was performed at the NSERC Guelph Regional STEM Facility (now named the Guelph Regional Integrated Imaging Facility), which is partially funded by an NSERC-Major Facility Access grant to T.J.B. Canada Research Chair funds and Canadian Foundation of Innovation funds to T.J.B. purchased the Leica EMPACT and EMAFS instrumentation.

REFERENCES

1. Abeyrathne, P. D., C. Daniels, K. K. H. Poon, M. J. Matewish, and J. S. Lam. 2005. Functional characterization of WaaL, a ligase associated with linking O-antigen polysaccharide to the core of *Pseudomonas aeruginosa* lipopolysaccharide. *J. Bacteriol.* **187**:3002–3012.
2. Arsenault, S. F., D. W. Hughes, D. B. McLean, W. A. Szarek, A. M. B. Kropinski, and J. S. Lam. 1991. Structural studies on the polysaccharide portion of 'A-band' lipopolysaccharide from a mutant (AK1401) of *Pseudomonas aeruginosa* strain PAO1. *Can. J. Chem.* **69**:1273–1280.
3. Bayer, M. E. 1990. Visualization of the bacterial polysaccharide capsule, p. 129–157. In K. Jann and B. Jann (ed.), *Bacterial capsules*. Springer-Verlag, New York, N.Y.
4. Beveridge, T. J. 1988. Wall ultrastructure; how little we know, p. 3–20. In P. Actor, L. Daneo-Moore, M. L. Higgins, M. R. J. Salton, and G. D. Shockman (ed.), *Antibiotic inhibition of bacteria cell surface assembly and function*. ASM Press, Washington, D.C.
5. Beveridge, T. J. 1999. Structures of gram-negative cell walls and their derived membrane vesicles. *J. Bacteriol.* **181**:4725–4733.
6. Beveridge, T. J. 2001. Use of the Gram stain in microbiology. *Biotechnol. Histochem.* **76**:111–118.
7. Beveridge, T. J., and V. R. F. Matias. Ultrastructure of the gram-positive cell wall. In V. A. Fischetti, R. P. Novick, J. J. Ferreti, D. A. Portnov, and J. I. Rood (ed.), *Gram-positive pathogens*, 2nd ed., in press. ASM Press, Washington, D.C.
8. Beveridge, T. J., S. A. Makin, J. L. Kadurugamuwa, and Z. Li. 1997. Interactions between biofilms and the environment. *FEMS Microbiol.* **20**:291–303.
9. Beveridge, T. J., J. R. Lawrence, and R. G. E. Murray. Sampling and staining for light microscopy. In C. A. Reddy, T. J. Beveridge, J. A. Breznak, L. Snyder, T. M. Schmidt, and G. A. Marzluf (ed.), *Methods for general and molecular microbiology*, 2nd ed., in press. ASM Press, Washington, D.C.

10. Beveridge, T. J., D. Moyles, and R. Harris. Electron microscopy. In C. A. Reddy, T. J. Beveridge, J. A. Breznak, L. Snyder, T. M. Schmidt, and G. A. Marzluf (ed.), *Methods for general and molecular microbiology*, 2nd ed., in press. ASM Press, Washington, D.C.
11. Branda, S. S., A. Vik, L. Friedman, and R. Kolter. 2005. Biofilms: the matrix revisited. *Trends Microbiol.* **13**:20–26.
12. Costerton, J. W., G. G. Geesey, and K.-J. Cheng. 1978. How bacteria stick. *Sci. Am.* **238**:86–95.
13. Costerton, J. W., Z. Lewandowski, D. E. Caldwell, D. R. Korber, and H. M. Lappin-Scott. 1995. Microbial biofilms. *Annu. Rev. Microbiol.* **49**:711–745.
14. Danilatos, G. D. 1993. Introduction to the ESEM instrument. *Microsc. Res. Tech.* **25**:354–361.
15. Dubochet, J., and N. Sartori Blanc. 2001. The cell in absence of aggregation artifacts. *Micron* **32**:91–99.
16. Dubochet, J., M. Adrian, J. J. Chang, J. C. Homo, J. Lepault, A. W. McDowell, and P. Schultz. 1988. Cryo-electron microscopy of vitrified specimens. *Q. Rev. Biophys.* **21**:129–228.
17. Eighmy, T. T., D. Maratea, and P. L. Bishop. 1983. Electron microscopic examination of wastewater biofilm formation and structural components. *Appl. Environ. Microbiol.* **45**:1921–1931.
18. Friedman, L., and R. Kolter. 2004. Genes involved in matrix formation in *Pseudomonas aeruginosa* PA14 biofilms. *Mol. Microbiol.* **51**:675–690.
19. Friedman, L., and R. Kolter. 2004. Two genetic loci produce distinct carbohydrate-rich structural components of the *P. aeruginosa* biofilm matrix. *J. Bacteriol.* **186**:4457–4465.
20. Geesey, G. G., W. T. Richardson, H. G. Yeomans, R. T. Irvin, and J. W. Costerton. 1977. Microscopic examination of natural sessile bacterial populations from an alpine stream. *Can. J. Microbiol.* **23**:1733–1736.
21. Graham, L. L. 1992. Freeze-substitution studies of bacteria. *Electron Microsc. Rev.* **5**:77–103.
22. Graham, L. L., and T. J. Beveridge. 1990. Evaluation of freeze-substitution and conventional embedding protocols for routine electron microscopic processing of eubacteria. *J. Bacteriol.* **172**:2141–2149.
23. Graham, L. L., and T. J. Beveridge. 1990. Effect of chemical fixatives on accurate preservation of *Escherichia coli* and *Bacillus subtilis* structure in cells prepared by freeze-substitution. *J. Bacteriol.* **172**:2150–2159.
24. Graham, L. L., and T. J. Beveridge. 1994. Structural differentiation of the *Bacillus subtilis* cell wall. *J. Bacteriol.* **176**:1413–1421.
25. Graham, L. L., R. Harris, W. Villiger, and T. J. Beveridge. 1991. Freeze-substitution of gram-negative eubacteria: general cell morphology and envelope profiles. *J. Bacteriol.* **173**:1623–1633.
26. Hitchcock, P. J., and T. M. Brown. 1983. Morphological heterogeneity among *Salmonella* lipopolysaccharide chemotypes in silver-stained polyacrylamide gels. *J. Bacteriol.* **154**:269–277.
27. Hobot, J. A., E. Carlemalm, W. Villiger, and E. Kellenberger. 1984. Periplasmic gel: new concept resulting from the reinvestigation of bacterial cell envelope ultrastructure by new methods. *J. Bacteriol.* **160**:143–152.
28. Hobot, J. A., M. A. Bjornsti, and E. Kellenberger. 1987. Use of on-section immunolabeling and cryosubstitution for studies of bacterial DNA distribution. *J. Bacteriol.* **169**:2055–2062.
29. Holt, S. C., and T. J. Beveridge. 1982. Electron microscopy: its development and application to microbiology. *Can. J. Microbiol.* **28**:1–53.
30. Hunter, R. C., and T. J. Beveridge. 2005. Application of a pH-sensitive fluorophore (C-SNARF-4) for pH microenvironment analysis in *Pseudomonas aeruginosa* biofilms. *Appl. Environ. Microbiol.* **75**:2501–2510.
31. Jacques, M., and M. Gottschalk. 1997. Use of monoclonal antibodies to visualize capsular material of bacterial pathogens by conventional electron microscopy. *Microsc. Microanal.* **3**:234–238.
32. Kamper, M., S. Vetterkind, R. Berker, and M. Hoppert. 2004. Methods for in situ detection and characterization of extracellular polymers by electron microscopy. *J. Microbiol. Methods* **57**:55–64.
33. Karlyshev, A. Y., M. V. McCrossan, and B. W. Wren. 2001. Demonstration of polysaccharide capsule in *Campylobacter jejuni* using electron microscopy. *Infect. Immun.* **69**:5921–5924.
34. Karthikeyan, S., and T. J. Beveridge. 2002. *Pseudomonas aeruginosa* can react with and precipitate toxic soluble gold. *Environ. Microbiol.* **4**:667–675.
35. Knirel, Y. A., E. V. Vinogradov, N. A. Kocharova, N. A. Paramonov, N. K. Kochetkov, B. A. Dmitriev, E. S. Stanislavsky, and B. Lanyi. 1988. The structure of O-specific polysaccharide and serological classification of *Pseudomonas aeruginosa*. *Acta Microbiol. Hung.* **35**:3–24.
36. Koval, S. F., and T. J. Beveridge. 1999. Electron microscopy, p. 276–287. In J. Lederberg (ed.), *Encyclopedia of microbiology*. Academic Press, San Diego, Calif.
37. Kreft, J.-U. 2004. Biofilms promote altruism. *Microbiology* **150**:2751–2760.
38. Lam, J. S., R. Chan, K. Lam, and J. W. Costerton. 1980. Production of mucoid microcolonies by *P. aeruginosa* within infected lungs in cystic fibrosis. *Infect. Immun.* **28**:546–556.
39. Lam, J. S., L. A. MacDonald, M. Y. C. Lam, L. G. M. Duchesne, and G. G. Southam. 1987. Production and characterization of monoclonal antibodies against serotype strains of *Pseudomonas aeruginosa*. *Infect. Immun.* **55**:1051–1057.
40. Lam, M. Y. C., E. J. McGroarty, A. M. Kropinski, L. A. MacDonald, S. S. Pedersen, N. Hoiby, and J. S. Lam. 1989. Occurrence of a common lipopolysaccharide antigen in standard and clinical strains of *Pseudomonas aeruginosa*. *J. Clin. Microbiol.* **27**:962–967.
41. Lam, J. S., L. L. Graham, J. Lightfoot, T. Dasgupta, and T. J. Beveridge. 1992. Ultrastructural examination of the lipopolysaccharides of *Pseudomonas aeruginosa* strains and their isogenic rough mutants by freeze-substitution. *J. Bacteriol.* **174**:7159–7167.
42. Langley, S., and T. J. Beveridge. 1999. Metal binding by *Pseudomonas aeruginosa* PAO1 is influenced by growth of the cells as a biofilm. *Can. J. Microbiol.* **45**:616–622.
43. Lawrence, J. R., and T. R. Neu. Laser scanning microscopy. In C. A. Reddy, T. J. Beveridge, J. A. Breznak, L. Snyder, T. M. Schmidt, and G. A. Marzluf (ed.), *Methods for general and molecular microbiology*, 2nd ed., in press. ASM Press, Washington, D.C.
44. Lawrence, J. R., D. R. Korber, B. D. Hoyle, J. W. Costerton, and D. E. Caldwell. 1991. Optical sectioning of microbial biofilms. *J. Bacteriol.* **173**:6558–6567.
45. Lawrence, J. R., G. D. W. Swerhone, G. G. Leppard, T. Araki, X. Zhang, M. M. West, and A. P. Hitchcock. 2003. Scanning transmission X-ray, laser scanning, and transmission electron microscopy mapping of the exopolymeric matrix of microbial biofilms. *Appl. Environ. Microbiol.* **69**:5543–5554.
46. Lazazzera, B. A. 2005. Lessons from DNA microarray analysis: the gene expression profile of biofilms. *Curr. Opin. Microbiol.* **8**:222–227.
47. Lee, J.-U., and T. J. Beveridge. 2001. Interaction between iron and *Pseudomonas aeruginosa* biofilms attached to Sepharose surfaces. *Chem. Geol.* **180**:67–80.
48. Luft, J. H. 1971. Ruthenium red and violet. I. Chemistry, purification, methods of use for electron microscopy and mechanism of action. *Anat. Rec.* **171**:347–368.
49. Makin, S. A., and T. J. Beveridge. 1996. The influence of A-band and B-band lipopolysaccharide on the surface characteristics and adhesion of *Pseudomonas aeruginosa* to surfaces. *Microbiology* **142**:299–307.
50. Matias, V. R. F., and T. J. Beveridge. 2005. Cryo-electron microscopy reveals native polymeric cell wall structure in *Bacillus subtilis* 168 and the existence of a periplasmic space. *Mol. Microbiol.* **56**:240–251.
51. Matias, V. R. F., A. Al-Amoudi, J. Dubochet, and T. J. Beveridge. 2003. Cryo-transmission electron microscopy of frozen-hydrated sections of *Escherichia coli* and *Pseudomonas aeruginosa*. *J. Bacteriol.* **185**:6112–6118.
52. Matsukawa, M., and E. P. Greenberg. 2004. Putative exopolysaccharide synthesis genes influence *Pseudomonas aeruginosa* biofilm development. *J. Bacteriol.* **186**:4449–4456.
53. McGroarty, E., and M. Rivera. 1990. Growth dependent alterations in production of serotype-specific and common antigen lipopolysaccharides in *Pseudomonas aeruginosa* PAO1. *Infect. Immun.* **58**:1030–1037.
54. Paul, T. R., and T. J. Beveridge. 1992. Reevaluation of envelope profiles and cytoplasmic ultrastructure of mycobacteria processed by conventional embedding and freeze-substitution protocols. *J. Bacteriol.* **174**:6508–6517.
55. Paul, T. R., and T. J. Beveridge. 1994. Preservation of surface lipids and determination of ultrastructure of *Mycobacterium kansasii* by freeze-substitution. *Infect. Immun.* **62**:1542–1550.
56. Phoenix, V., A. A. Korenevsky, V. R. F. Matias, and T. J. Beveridge. Cell wall structure and physicochemistry provide new insights into metal ion nucleation and mineral development in bacteria. In G. Gadd (ed.), *Microorganisms and earth systems: advances in geomicrobiology*, in press. Society for General Microbiology/Cambridge Press, Cambridge, United Kingdom.
57. Poulsen, L. K., G. Ballard, and D. A. Stahl. 1993. Use of rRNA fluorescence *in situ* hybridization for measuring the activity of single cells in young and established biofilms. *Appl. Environ. Microbiol.* **59**:1354–1360.
58. Rochetta, H. L., L. L. Burrows, and J. S. Lam. 1999. Genetics of O-antigen biosynthesis in *Pseudomonas aeruginosa*. *Microbiol. Mol. Biol. Rev.* **63**:523–553.
59. Sabra, W., H. Lunsdorf, and A. P. Zeng. 2003. Alterations in the formation of lipopolysaccharide and membrane vesicles on the surface of *Pseudomonas aeruginosa* PAO1 under oxygen stress conditions. *Microbiology* **149**:2789–2795.
60. Schembri, M. A., K. Kjaergaard, and P. Klemm. 2003. Global gene expression in *Escherichia coli* biofilms. *Mol. Microbiol.* **48**:253–267.
61. Scott, J. E., G. Quintarelli, and M. C. Dellovo. 1964. The chemical and histochemical properties of alcian blue. I. The mechanism of Alcian blue staining. *Histochemie* **4**:73–85.
62. Stanley, N. R., R. A. Britton, A. D. Grossman, and B. A. Lazazzera. 2003. Identification of catabolite repression as a physiological regulator of biofilm formation by *Bacillus subtilis* by use of DNA microarrays. *J. Bacteriol.* **185**:1951–1957.
63. Studer, D., W. Graber, A. Al-Amoudi, and P. Egli. 2001. A new approach for cryofixation by high-pressure freezing. *J. Microsc.* **203**:285–294.
64. Sutherland, I. W. 2001. The biofilm matrix – an immobilized but dynamic microbial environment. *Trends Microbiol.* **9**:222–227.

65. Vroom, J. M., K. J. De Grauw, H. C. Gerritsen, D. J. Bradshaw, P. D. Marsh, G. K. Watson, J. J. Birmingham, and C. Allison. 1999. Depth penetration and detection of pH gradients in biofilms by two-photon excitation microscopy. *Appl. Environ. Microbiol.* **65**:3502–3511.
66. Walters, M. C., F. Roe, A. Bugnicourt, M. J. Franklin, and P. S. Stewart. 2003. Contributions of antibiotic penetration, oxygen limitation, and low metabolic activity to tolerance of *Pseudomonas aeruginosa* biofilms to ciprofloxacin and tobramycin. *Antimicrob. Agents Chemother.* **47**:317–323.
67. Webster, P., S. Wu, S. Webster, K. A. Rich, and K. McDonald. 2004. Ultrastructural preservation of biofilms formed by a non-typable *Haemophilus influenzae*. *Biofilms* **1**:165–182.
68. Whitchurch, C. B., T. Tolker-Nielsen, P. C. Ragas, and J. S. Mattick. 2002. Extracellular DNA required for bacterial biofilm formation. *Science* **295**:1487.
69. Whiteley, M., M. G. Banger, R. E. Bumgarner, M. R. Parsek, G. M. Teitzel, S. Lory, and E. P. Greenberg. 2001. Gene expression in *Pseudomonas aeruginosa* biofilms. *Nature* **413**:860–864.
70. Wozniak, D. J., T. J. O. Wyckoff, M. Starkey, R. Keyser, P. Azadi, G. A. O'Toole, and M. R. Parsek. 2003. Alginate is not a significant component of the extracellular polysaccharide matrix of PA14 and PAO1 *Pseudomonas aeruginosa* biofilms. *Proc. Natl. Acad. Sci. USA*. **100**:7907–7912.
71. Yidliz, F. H., and G. K. Schoolnik. 1999. *Vibrio cholerae* O1 El Tor: Identification of a gene cluster required for the rugose colony type, exopolysaccharide production, chlorine resistance, and biofilm formation. *Proc. Natl. Acad. Sci. USA*. **96**:4028–4033.
72. Zahller, J., and P. S. Stewart. 2002. Transmission electron microscopy of antibiotic action on *Klebsiella pneumoniae* biofilm. *Antimicrob. Agents Chemother.* **46**:2679–2683.